

Nonlinear Cyclotron Resonance Absorber for a Microwave Subnanosecond Pulse Generator Powered by a Helical-Waveguide Gyrotron Traveling-Wave Tube

N. S. Ginzburg[✉], G. G. Denisov, M. N. Vilkov, A. S. Sergeev, S. V. Samsonov, A. M. Malkin, and I. V. Zotova

Institute of Applied Physics RAS, Nizhny Novgorod, Russia



(Received 11 June 2019; revised manuscript received 31 January 2020; accepted 17 March 2020; published 13 April 2020)

A well-known principle for periodical production of high-power ultrashort optical pulses is related to passive mode locking realized when a saturable absorber is incorporated into the laser resonator. A similar effect can be implemented in two-section electronic oscillators comprising an amplifier and a saturable absorber, which should be applicable in the microwave frequency band and suitable for high-power operation. In this paper, we analyze in detail the possibility of realizing a saturable absorber based on cyclotron resonance interaction in the regular waveguide with initially rectilinear electron beam, when saturation is caused by the relativistic dependence of the gyrofrequency on electron energy. Maximum contrast between the absorption of a high-power signal and of a weak signal is achieved in the group synchronism regime when the particle velocity is close to the wave's group velocity. Within the frame of a time-domain self-consistent model, we demonstrate that when such an absorber is installed in the feedback loop of an electron generator powered by existing Ka-band helical-waveguide gyrotron traveling-wave tube, periodical generation of subnanosecond pulses can be provided with peak power up to several hundred kW and sub-GHz repetition frequency. We discuss the influence of deviation from the group synchronism regime on the parameters of generated pulses. Experimental feasibility of the considered scheme is verified based on three-dimensional particle-in-cell simulations.

DOI: [10.1103/PhysRevApplied.13.044033](https://doi.org/10.1103/PhysRevApplied.13.044033)

I. INTRODUCTION

Development of microwave generators providing periodical trains of short (subnanosecond) pulses is motivated by a large number of fundamental problems and practical applications including high-resolution nanosecond radars, studying the physics of electrical explosions of conductors and detonation processes, high-gradient acceleration of charged particles, photochemistry, biophysics, and spectroscopy of various media [1–3]. In particular, significant improvement of functionality (in terms of sensitivity, resolution, data acquisition speed, etc.) of dynamic nuclear polarization-enhanced nuclear magnetic resonance (DNP NMR) spectroscopy, as well as other methods of monitoring the various media (e.g., dense plasma diagnostic) can be achieved using millimeter- and submillimeter-range radiation sources with controllable spectra. Requirements on the spectrum control include not only smooth sweep of the center frequency over a wide range, but also periodical short phase-correlated pulse generation with adjustable repetition rate. It should be noted that the spectrum of such radiation represents the so-called “frequency comb” demanded in wide-range resonator spectroscopy [3]. This method allows useful information to be rapidly

obtained about the substance filling the resonator. Such an approach is promising for control of technological processes, solving the problems of environmental safety, countering manmade threats etc.

Similarly to laser physics, periodical generation of short electromagnetic pulses in electron devices can be provided using active and passive mode-locking techniques. Active mode locking is provided by periodical modulation of electron current or resonator quality factor, which can be referred to as I switching or Q switching, respectively. For example, I switching is widely used in free-electrons lasers (FELs) operating in terahertz or infrared bands [4–6]. Such a FEL is driven by a periodical train of relativistic (10–100 MeV) short electron bunches formed with a MHz repetition rate. For mode-locking realization, the distance between the resonator's mirrors is chosen so that the repetition period of the current pulses is close to the roundtrip time of the electromagnetic pulse through the resonator. In the microwave range, active I -switching mode locking in gyrotrons was theoretically described in Ref. [7].

Q switching was proposed and experimentally realized in microwave FELs [8,9] based on a $p-i-n$ diode modulator. An alternative scheme of Q switching using “semiconductor-metal” phase transition in a plate periodically irradiated by laser pulses was theoretically studied for a backward-wave oscillator in Ref. [10]. In both cases,

* ginzburg@appl.sci-nnov.ru

the modulating signal is forced at a frequency that corresponds to the rf roundtrip time in the cavity or the feedback loop. However, these methods are limited in terms of the output power due to inclusion of solid-state elements into the feedback loop.

For realization of passive mode locking in laser physics [11–14], a saturable absorber or Kerr lens [14] is incorporated into the laser resonator. This technique allows for the generation of light pulses with picosecond and femtosecond durations needed in the broad domain of applications ranging from optical-fiber communication [15,16] and molecular spectroscopy [17] to petawatt laser complexes [18,19]. In Refs. [20,21], it was shown that a similar method of pulse generation can be implemented in high-power microwave electronics by incorporating a broadband electron amplifier and a saturable absorber into the feedback loop.

A basic requirement of the amplifying unit is the broad frequency bandwidth demanded for effective amplification of short microwave pulses. In the millimeter wavelength bands, it is attractive to utilize a type of gyrotron traveling-wave tube (gyro TWT) with a helically corrugated waveguide [22–27]. Such gyro TWTs possess a number of unique features, including broad amplification bandwidth up to 10%–15%. Note that this value determines the spectrum width of microwave radiation, which, similarly to optics, remains significantly smaller than the carrier frequency. Thus, the considered scheme can provide subnanosecond duration of the generated pulses. Such pulses can be referred to as “microwave ultrashort pulses” as a result of proper scaling of a femtosecond optical pulse duration to microwaves.

At the moment, the key problem for development of microwave mode-locked generators is the realization of the nonlinear absorber applicable to the microwave frequency band and suitable for high-power operation. In Ref. [21], we considered a scheme with an auxiliary helical-waveguide gyro TWT operating in the Kompfner dip regime (cf. Refs. [28,29]). An advantage of such an absorber is operation at the second cyclotron harmonic with a relatively low magnetic field. However, for microwave short-pulse generation with wideband spectrum, the rotating beam providing the Kompfner absorption in the center of the signal bandwidth would facilitate undesirable amplification at the frequencies further away from the spectrum maximum. As the additional analysis shows, this can lead to parasitic self-excitation of the system.

As suggested in Ref. [30], an alternative variant of the absorber can be based on the interaction of radiation at the fundamental cyclotron harmonic with an initially rectilinear electron beam guided by a resonance magnetic field. Saturation of absorption in this case is caused by relativistic dependence of the gyrofrequency on electrons energy [31]. Such an operation at the fundamental harmonic

would require a magnetic field two times higher than that in the case of the Kompfner absorber with the same frequency. However, using an initially rectilinear electron beam looks beneficial to avoid spurious self-excitation in the entire frequency range.

This paper contains the detailed theoretical analysis of a mode-locked electron generator comprising a helical-waveguide gyro TWT and a cyclotron resonance absorber. This scheme is to be used in “proof-of-principle” Ka-band experiments. In Sec. II, we develop a self-consistent time-domain model for theoretical description of the considered scheme. Based on the model, regimes of periodical generation of subnanosecond pulses are studied in Sec. III with parameters of the experimentally realized Ka-band gyro TWT [27]. Dependence of output parameters and operating regimes on deviation from the regime of group synchronism with the operating mode in the absorber is discussed. Results of Sec. III form a benchmark for full-scale three-dimensional (3D) particle-in-cell (PIC) simulations presented in Sec. IV, which took into account a number of additional real-life factors (including the input and output coupling, spatial charge influence, etc.). The full-scale model confirmed, in particular, the stability of the proposed system to spurious self-excitation.

II. TIME-DOMAIN MODEL OF MODE-LOCKED ELECTRON GENERATOR WITH CYCLOTRON RESONANCE ABSORBER

The principal scheme of the considered microwave mode-locked generator is presented in Fig. 1(a). The generator includes two coupled units, namely, a gyro-TWT amplifier (index “1”) and a saturable cyclotron resonance absorber (index “2”) driven by independent electron beams. Delayed feedback is provided by a partially transparent mirror. A detailed scheme describing the main features of the experimental setup is presented in Fig. 1(b). The amplifying section in the form of a helically corrugated waveguide is fed by a rotating electron beam, which excites the operating mode at the second harmonic of the gyrofrequency. In the absorbing section with a regular cylindrical waveguide, an initially rectilinear electron beam interacting with electromagnetic field at the fundamental cyclotron harmonic is used. The sections are coupled through the system of polarizers, which allow for energy extraction (see in detail Sec. IV). Note that in this section we construct an averaged time-domain model with a simplified variant of the generator scheme in which transitions between sections is described by equivalent boundary conditions corresponding to a partially transparent mirror.

Following Ref. [22], we assume that multifold helical corrugation in the amplifying section 1 is given by $r(\varphi, z) = r_1 + \tilde{r} \cos(\tilde{m}\varphi - \tilde{h}z)$, where r_1 is the waveguide mean radius, \tilde{r} and d are the corrugation amplitude and

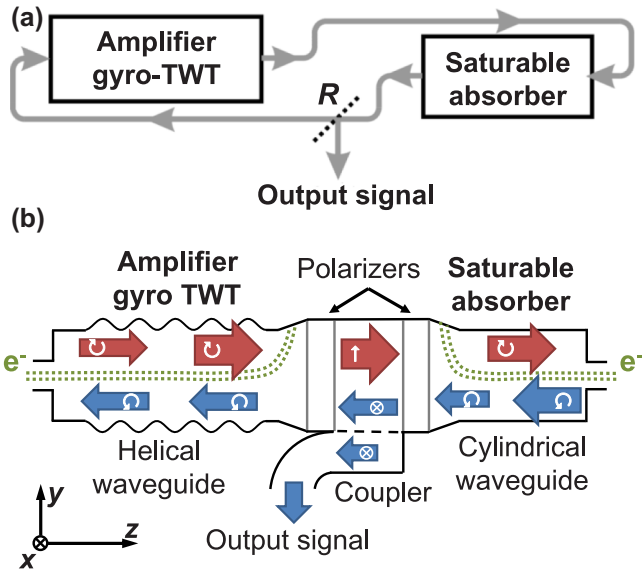


FIG. 1. (a) Flow diagram of a microwave mode-locked generator comprising a helical-waveguide gyro TWT (amplifier) and a regular-waveguide saturable cyclotron resonance absorber. (b) 3D PIC computer model reflecting the main features of the experimental setup: independent e-beams both in the amplifier and in the absorber interact with co-traveling circularly polarized waves; within the space between the polarizers, the opposite-propagating waves are polarized linearly orthogonal to each other; the polarization-selective coupler couples out only the x-polarized wave.

period, \bar{m} is the number of corrugation folds, $\bar{h} = 2\pi/d$. Under the Bragg resonance conditions $\bar{m} = m_A - m_B$, $\bar{h} \approx h_B$, such corrugation provides coupling of two rotating TE _{m,n} modes of a unperturbed cylindrical waveguide, the first of which is quasicutoff (A), while the second one is a traveling wave (B). Here $m_{A,B}$ are the azimuthal modes' indices and h_B is the longitudinal wave number of the mode B ($h_A \rightarrow 0$). Electrical fields of the partial waves can be presented in the form:

$$\vec{E}_A = \text{Re}[A(z, t)\vec{E}_\perp^A(r)e^{i(\omega_A t - m_A \varphi)}], \quad (1)$$

$$\vec{E}_B = \text{Re}[B(z, t)\vec{E}_\perp^B(r)e^{i(\omega_A t - h_0 z - m_B \varphi)}],$$

where $A(z, t)$ and $B(z, t)$ are the slowly varying amplitudes, $\vec{E}_\perp^A(r)$ and $\vec{E}_\perp^B(r)$ are the radial structures of the partial waves, ω_A is the cutoff frequency of the mode A chosen as a reference one. The mentioned pair of waveguide modes is selectively excited at the s th gyrofrequency harmonic by an axis-encircling rotating electron beam under cyclotron resonance conditions

$$\omega \approx \omega_A \approx s\omega_{H1}, \quad (2)$$

where $\omega_{H1} = eH_1/m_e c \gamma_1$ is the relativistic gyrofrequency, H_1 is the guiding magnetic field in the amplifying unit, γ_1 is the Lorentz factor.

Representing the field amplitude in the form $A, B = \int (A_\Omega, B_\Omega) e^{i\Omega t} d\Omega$ ($\Omega = \omega - \omega_A$ is the detuning of the radiation frequency $\omega = 2\pi f$ from the carrier cutoff frequency ω_A), we can describe the amplification of spectral components $A_\Omega, B_\Omega = (2\pi)^{-1} \int (A, B) e^{-i\Omega t} dt$ using the system of coupled ordinary differential equations, which were derived for cw regimes in Ref. [23]:

$$\begin{aligned} \frac{d^2 \hat{A}_\Omega}{dz^2} + 2 \frac{\omega_A \Omega}{c^2} \hat{A}_\Omega &= 2\sigma \frac{\omega_A^2}{c^2} \hat{B}_\Omega + J_\Omega, \\ i h_0 \frac{d \hat{B}_\Omega}{dz} - \left[\frac{\omega_A \Omega}{c^2} - h_0 (\bar{h} - h_0) \right] \hat{B}_\Omega &= -\sigma \frac{\omega_A^2}{c^2} \hat{A}_\Omega. \end{aligned} \quad (3)$$

Here $\hat{A}_\Omega = eA_\Omega \sqrt{N_A}/m_e c \omega_A$, $\hat{B}_\Omega = eB_\Omega \sqrt{N_B}/m_e c \omega_B$, $N_{A,B} = (v_{A,B}^2 - m_{A,B}^2) J_{m_{A,B}}^2(v_{A,B})$ are the dimensionless norms of the partial waves. J_m is the Bessel function, $v_A = \omega_A r_1/c$ and $v_B = \omega_B r_1/c$ are the roots of the equations $J'_{m_A}(v_A) = J'_{m_B}(v_B) = 0$, ω_B is the cutoff frequency of the traveling mode B , $h_0 = h_B(\omega_A) = \sqrt{\omega_A^2 - \omega_B^2}/c$, $\sigma = (\tilde{r}/2r_1) \left[(v_B^2 - m_A m_B) / \sqrt{(v_A^2 - m_A^2)(v_B^2 - m_B^2)} \right]$ is the coupling parameter obtained in the shallow corrugation approximation $r \ll \lambda$ [22], J_Ω is the Fourier harmonic of the normalized high-frequency component of the electron current. For signals with a narrow spectra in the scale of the carrier frequency $\Delta\omega/\omega \ll 1$, using the inverse Fourier transform, we obtain the following system of equations comprising the parabolic equation for quasicutoff mode A and the transport equation for traveling mode B [32]:

$$\begin{aligned} \frac{\partial^2 \hat{A}}{\partial z^2} - 2i \frac{\omega_A}{c^2} \frac{\partial \hat{A}}{\partial t} &= 2\sigma \frac{\omega_A^2}{c^2} \hat{B} + J, \\ \left(\frac{\partial}{\partial z} + \frac{1}{V_{\text{gr1}}} \frac{\partial}{\partial t} \right) \hat{B} - i(\bar{h} - h_0) \hat{B} &= i \frac{\omega_A^2}{c^2 h_0} \sigma \hat{A}, \end{aligned} \quad (4)$$

where $V_{\text{gr1}} = c\beta_{\text{gr1}} = h_0 c^2/\omega_A$ is the group velocity of mode B at the reference frequency ω_A . The electron current J in the right-hand side of the parabolic equation can be found in the same way as in the theory of gyrotrons [33] based on the motion equations for electrons,

$$\begin{aligned} J &= i \frac{8eI_1}{m_e c^3} \frac{\omega_A^2}{c^2 \beta_{||1} \sqrt{N_A}} \frac{s^s}{2^s s!} \frac{1}{2\pi} \int_0^{2\pi} p_1^s d\theta_0, \\ &\left(\frac{\partial}{\partial z} + \frac{1}{V_{||1}} \frac{\partial}{\partial t} \right) p_1 + i \frac{\omega_A}{2V_{||1}} \frac{p_1}{s} (\Delta_1 + |p_1|^2 - \beta_{||1}^2) \\ &= \frac{s^s}{2^s s!} \frac{\omega_A}{V_{||1} \sqrt{N_A}} \hat{A} (p_1^*)^{s-1}, \end{aligned} \quad (5)$$

where $p_1 = (p_{1x} + ip_{1y})e^{-i\omega_A t + i(m_A - s)\varphi}/m_e c$ is the normalized transverse electron momentum, $V_{||1} = c\beta_{||1}$ and $V_{\perp 1} = c\beta_{\perp 1}$ are the initial longitudinal and transverse electron velocities, I_1 is the amplifier's beam current, $\Delta_1 = 2(\omega_A - s\omega_{H1})/\omega_A$ is the cyclotron resonance detuning.

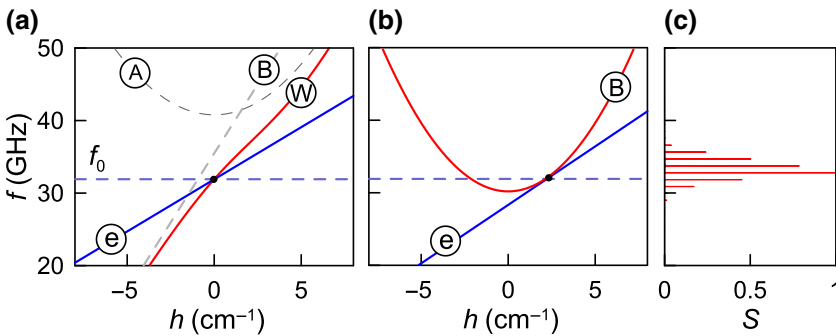
Putting down the boundary conditions for motion Eqs. (5), we assume that at the input of the amplifier, electrons of the rotating beam are uniformly distributed over cyclotron phases

$$p_1 = \beta_{\perp 1} e^{i\theta_0}, \quad \theta_0 \in [0, 2\pi). \quad (6)$$

For the quasicutoff wave A at the edges of the amplifier's interaction space z_{in} and z_{out} , we apply nonreflecting boundary conditions in the form [34]:

$$\begin{aligned} \left[\hat{A}(z, t) - \frac{c}{\sqrt{2\pi i\omega_A}} \int_0^t \frac{1}{\sqrt{t-t'}} \frac{\partial \hat{A}(z, t')}{\partial z} dt' \right] \Big|_{z_{\text{in}}} &= 0, \\ \left[\hat{A}(z, t) + \frac{c}{\sqrt{2\pi i\omega_A}} \int_0^t \frac{1}{\sqrt{t-t'}} \frac{\partial \hat{A}(z, t')}{\partial z} dt' \right] \Big|_{z_{\text{out}}} &= 0. \end{aligned} \quad (7)$$

After the amplifier, a traveling mode B enters the absorbing section 2, which has the form of a smoothly tapered regular waveguide driven by a magnetized initially rectilinear electron beam. Group synchronism regime of beam-wave interaction, which is beneficial for effective pulse generation (see Fig. 5 below), corresponds to the grazing between the beam line $\omega = hV_{||2} + \omega_{H2}$ (where h is the longitudinal wave number) and the dispersion characteristic of the operating mode [see Fig. 2(b)]. For weakly relativistic electrons, the frequency of the grazing point is close to the waveguide cutoff similarly to interaction regime in gyrotrons. Thus, the equations for the absorbing section follow from the well-known nonstationary gyrotron equations [34] for zero initial oscillatory velocity



of electrons.

$$\begin{aligned} i \frac{\partial^2 \hat{B}}{\partial z^2} + \frac{2\omega_{B2}^2}{c^2} \left(i\delta_2 + \frac{1}{\omega_{B2}} \frac{\partial}{\partial t} \right) \hat{B} &= \frac{4eI_2}{m_e c^3} \frac{\omega_{B2}^3}{c V_{||2} \omega_{B1} \sqrt{N_B}} p_2, \\ \left(\frac{\partial}{\partial z} + \frac{1}{V_{||2}} \frac{\partial}{\partial t} \right) p_2 + i \frac{\omega_{B2}}{2V_{||2}} p_2 (\Delta_2 + 2\delta_2 + |p_2|^2) \\ &= -\frac{\omega_{B1}}{2V_{||2} \sqrt{N_B}} \hat{B}, \end{aligned} \quad (8)$$

where $\omega_{B2} = cv_B/r_2$ is the cutoff frequency of an operating mode in the absorbing section, $p_2 = (p_{2x} + ip_{2y})e^{-i\omega_{A2} t + i(m_B - 1)\varphi}/m_e c$ is the normalized transverse electron momentum of the second electron beam, $\Delta_2 = 2(1 - \omega_{H2}/\omega_{B2})$ is the cyclotron resonance detuning, $\omega_{H2} = eH_2/m_e \gamma_2$ is the gyrofrequency, H_2 is the guiding magnetic field in the absorber, r_2 is the radius of the absorber waveguide, I_2 is the current of the absorber beam, $\delta_2 = \omega_A/\omega_{B2} - 1$. For initially rectilinear electron beam in the absorbing section, zero boundary condition at the input of the interaction space is used: $p_2 = 0$. Correspondingly, there is no averaging over initial phases of cyclotron rotation in the left part of the parabolic equation for field evolution [see Eq. (8)]. Note also that in the original gyrotron equations, the time derivative $V_{||2}^{-1} \partial / \partial t$ in the motion equation is typically neglected [34]; we retain this term in Eq. (8) as it is crucial for the description of the grazing regime [35].

In accordance with the scheme shown in Fig. 1(a), the signal from the output of the amplifier arrives at the input of the absorber without losses. Thus, the boundary conditions for the field amplitude \hat{B} in the input $z_{\text{in}}^{\text{abs}}$ and output $z_{\text{out}}^{\text{abs}}$ absorber cross sections can be written in the form [36]

$$\begin{aligned} \left[\hat{B}(z, t) - \frac{c}{\sqrt{2\pi i\omega_{B2}}} \int_0^t \frac{e^{-i\omega_{B2}\delta_2(t-t')}}{\sqrt{t-t'}} \frac{\partial \hat{B}(z, t')}{\partial z} dt' \right] \Big|_{z_{\text{in}}^{\text{abs}}} \\ = 2 \frac{\omega_{B2}}{\omega_{B1}} \sqrt{\frac{\beta_{\text{gr1}}}{\beta_{\text{gr2}}}} \hat{B}(z_{\text{in}}, t), \end{aligned}$$

FIG. 2. Dispersion diagrams in the amplifying (a) and absorbing (b) sections of the Ka-band mode-locked generator: (A),(B) are partial waves, (W) is the normal wave in the amplifying section, (e) is the electron-beam line. (c) Spectrum of output radiation.

$$\left[\hat{B}(z, t) + \frac{c}{\sqrt{2\pi i\omega_{B2}}} \int_0^t \frac{e^{-i\omega_{B2}\delta_2(t-t')}}{\sqrt{t-t'}} \frac{\partial \hat{B}(z, t')}{\partial z} dt' \right] \Big|_{z_{\text{out}}^{\text{abs}}} = 0. \quad (9)$$

From the output of the absorber, the signal returns to the input of the amplifier with the transmission coefficient R and the delay time t_d , so

$$\hat{B}(z_{\text{in}}, t) = R \frac{\omega_{B1}}{\omega_{B2}} \sqrt{\frac{\beta_{\text{gr2}}}{\beta_{\text{gr1}}}} \hat{B}(z_{\text{out}}^{\text{abs}}, t - t_d), \quad (10)$$

where

$$V_{\text{gr2}} = c\beta_{\text{gr2}} = (dh/d\omega|_{\omega=\omega_g})^{-1} = c\sqrt{2(\omega_g - \omega_{B2})/\omega_{B2}}$$

is the group velocity of the operating wave in the absorber,

$$\omega_g = \omega_A + 0.5 \left[\beta_{\text{gr1}}(\bar{h} - h_0) - \sqrt{\beta_{\text{gr1}}^2(\bar{h} - h_0)^2 + 4\sigma^2\omega_A^2/c^2} \right]$$

the frequency of the normal wave of the helically corrugated waveguide at zero longitudinal wave number, which determines the central frequency of the spectrum in the regime of pulse generation.

The output useful power of the mode-locked generator is given by relation

$$P = \frac{m_e^2 c^5}{8e^2} \frac{c\omega_{B1}^2}{\omega_{B2}^3} (1 - R^2) \left| \text{Im} \left(\hat{B} \frac{\partial \hat{B}^*}{\partial z} \right) \right|_{z=z_{\text{out}}^{\text{abs}}}. \quad (11)$$

The efficiency of the amplifier unit can be found as

$$\eta_1 = \frac{g^2}{1+g^2} \eta_{\perp}, \quad \eta_{\perp} = 1 - \frac{1}{2\pi} \int_0^{2\pi} \frac{|p_1(z_{\text{out}})|^2}{\beta_{\perp 1}^2} d\theta_0, \quad (12)$$

where $g = V_{\perp 1}/V_{||1}$ is the pitch factor of the rotating electron beam. The absorption (energy consumption) ratio in section 2 can be characterized by

$$\eta_2 = -|p_2(z_{\text{out}}^{\text{abs}})|^2. \quad (13)$$

III. RESULTS OF SIMULATIONS

In simulations, parameters of the amplifying unit (Fig. 1) are chosen to be close to the parameters of the experimentally realized Ka-band gyro TWT [27], in which a threefold helical corrugation is used for coupling of near-cutoff TE_{2,1} to counterrotating traveling TE_{-1,1} modes. The resulting normal mode is excited at the second cyclotron harmonic ($s = 2$) by an encircling rotating electron beam with a particle energy of 68–70 keV, total current of 8–10 A, and pitch factor of 1.2. As shown in Ref. [32], efficient amplification of short (subnanosecond) electromagnetic pulses is achieved under the condition of intersection between the beam line $\omega = hV_{||1} + s\omega_{H1}$ and

the dispersion characteristic of the normal wave W . In this case, due to the difference between the wave's group velocity and the axial velocity of the electrons, electromagnetic pulse accumulates the energy from different fractions of the electron beam in the process of the slippage of the pulse over the electrons. Dispersion relation of the normal wave W in the helically corrugated waveguide can be put down in the form [23]

$$[2\omega_A(\omega - \omega_A) - h^2 c^2] \left(\frac{\omega - \omega_A}{V_{\text{gr1}}} - \bar{h} + h_0 - h \right) = \frac{2\sigma^2 \omega_A^4}{h_0 c^2}. \quad (14)$$

In the absorbing unit, the optimal regime corresponds to grazing (instead of intersection) between the beam line $\omega = hV_{||2} + \omega_{H2}$ and the dispersion characteristic of the operating mode B

$$2\omega_{B2}(\omega - \omega_{B2}) = h^2 c^2. \quad (15)$$

In this case the electron axial velocity is equal to the group velocity of the wave (so-called group synchronism regime), thus the mutual influence of different parts of a single electromagnetic pulse is minimized. Such a system is equivalent to absorbers with fast response time (for example, Kerr cells [14]) used in mode-locked lasers.

In Figs. 2(a) and 2(b), dispersion diagrams for the amplifying and the absorbing sections are presented for parameters summarized in Table I. For amplifier guiding magnetic field $H_1 = 0.64$ T, the resonant point corresponds to the central frequency of the electromagnetic pulse $f_0 = 32$ GHz. The grazing regime in the absorber is provided for the guiding magnetic field of $H_0 = 1.08$ T. Saturation of absorption is demonstrated in Fig. 3: small-amplitude signals are strongly damped while signals with larger amplitudes transmit without visible attenuation. For cyclotron absorption, such bleaching is caused by relativistic dependence of gyrofrequency on electron energy.

TABLE I. Parameters of amplifying and absorbing sections in soft-excitation regime with maximum peak power of generated pulses.

| | Amplifier | Absorber |
|-----------------------|---------------------------------------|--------------------|
| Electron energy | 68 keV | 32 keV |
| Electron current | 10 A | 3.8 A |
| Pitch factor | 1.2 | 0 |
| Interaction length | 18.4 cm | 3 cm |
| Waveguide radius | 0.36 cm | 0.29 cm |
| Corrugation period | 1.16 cm | — |
| Corrugation amplitude | 0.7 cm | — |
| Operating mode | TE _{2,1} /TE _{-1,1} | TE _{-1,1} |

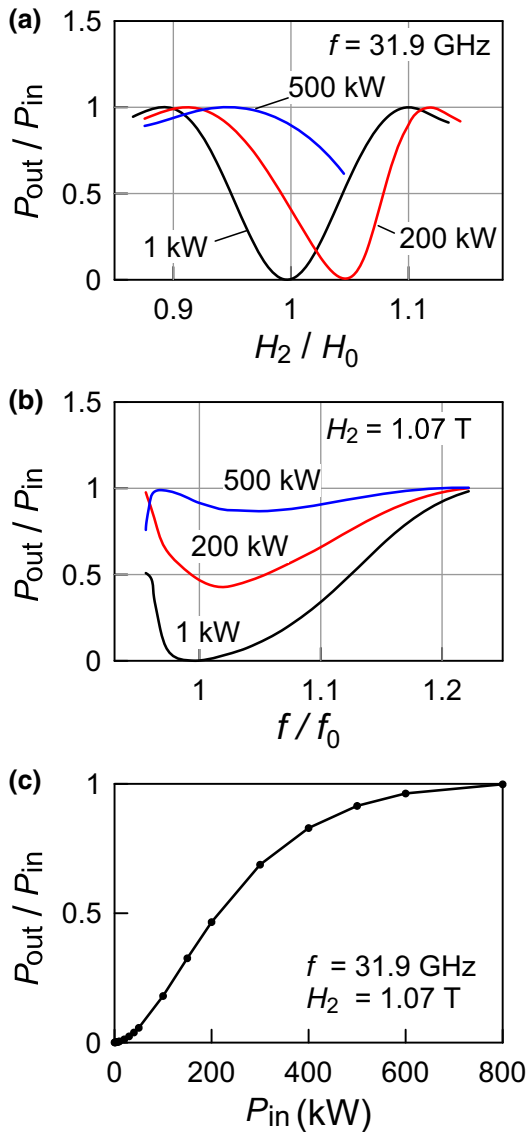


FIG. 3. Demonstration of absorption saturation. Dependences of the transmission coefficient of the cyclotron absorber (a) on the value of the guiding magnetic field, (b) on the frequency of the incident signal, and (c) on the input power.

For a transmission coefficient of 0.3 and delay time of 2.6 ns, soft-excitation regime of periodical pulse generation in the two-section oscillator is observed in simulations (Fig. 4). Spatial-temporal dynamics of the field amplitude in the amplifying and absorbing sections are shown in Fig. 5. Pulses generated with a repetition frequency of 1 GHz have subnanosecond duration (about 200 ps FWHM) and peak power of about 400 kW. The spectrum width reaches 3 GHz. Spectral lines correspond to eigenfrequencies of the feedback-loop modes.

It is important to note that the generated pulses are coherent, i.e., they have correlated phases, which is confirmed by calculations of a cross-correlation function for the single pulse $\hat{B}_1(t)$ and a complete pulses train $\hat{B}(t)$ with

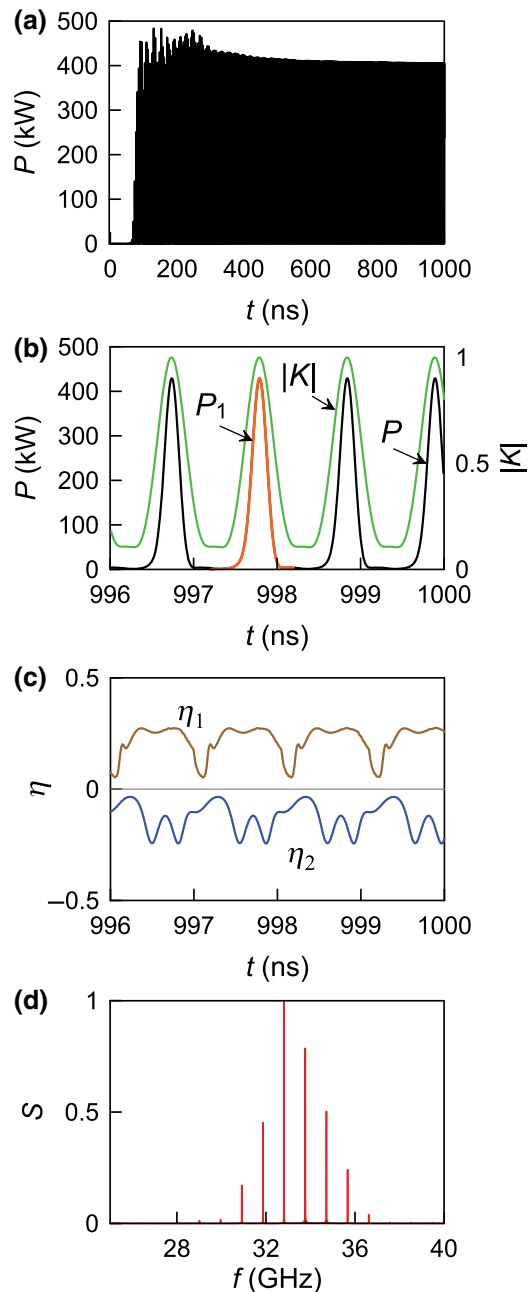


FIG. 4. Generation of the train of subnanosecond pulses in the electron mode-locked generator excited in a soft regime: (a) onset of the generation regime, (b) detailed profile of the generated pulses and the temporal dependence of the absolute value of the self-correlation function $K(t)$, where $P_1(t)$ is the test pulse, (c) temporal dependence of the orbital electron efficiency η_1 in the amplifier and the energy consumption ratio η_2 in the absorber, (d) the radiation spectrum.

period T :

$$K(t) = \frac{\int_0^T \hat{B}_1(t') \hat{B}^*(t' - t) dt'}{\left[\int_0^T |\hat{B}_1(t')|^2 dt' \cdot \int_{\tau}^{T+t} |\hat{B}(t')|^2 dt' \right]^{1/2}}. \quad (16)$$

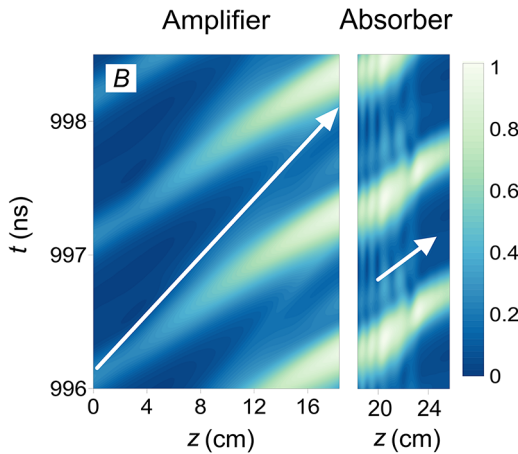


FIG. 5. Spatial-temporal dynamics of the field amplitude in the amplifying (a) and the absorbing (b) sections. White arrows correspond to electron characteristics. In the amplifier, the microwave pulse group velocity defers from the electrons' translational velocity, while in the absorber these velocities are equal (group synchronism, or grazing, regime).

As one can see in Fig. 4(b), the absolute value of this function reaches 1 at the pulses' repetition period.

It should be noted that the absorber's model, Eq. (8), with a time derivative in the motion equations allows the required accuracy of the beam-wave group synchronism to be estimated. In Fig. 6 (left column), variations of the pulses' profiles with changes in translational velocity of electrons in the absorber are shown. One can see that exact group synchronism ($V_{gr2} = V_{||2}$) in the absorber provides maximum peak power of stable microwave pulses, while a deviation from this regime leads to a decrease in the peak power and then to breakdown of generation. However, the microwave mode-locked generator has a certain tolerance for deviation from the grazing regime in the absorber, which is important for its experimental implementation. The magnetic field tuning corresponding to the grazing regime is also beneficial, as demonstrated in Fig. 6 (right column).

Obviously the considered two-section oscillator can exhibit several types of operation regimes for different combinations of parameters. Alongside soft excitation, there is hard-excitation regime when periodical pulse generation develops after injection of an external pulse into the system for bleaching of the absorber. In Fig. 7, hard-excitation regime is presented for parameters summarized in Table II, which also are reachable in experimental situation. Optimal values of the guiding magnetic field in the first and the second sections are $H_1 = 0.67$ T and $H_2 = 1.08$ T, respectively. According to simulations, generated pulses have duration of 250 ps (FWHM) and peak power of about 160 kW. Repetition frequency of 150 MHz corresponds to the whole pulse roundtrip time in the feedback loop of 6 ns.

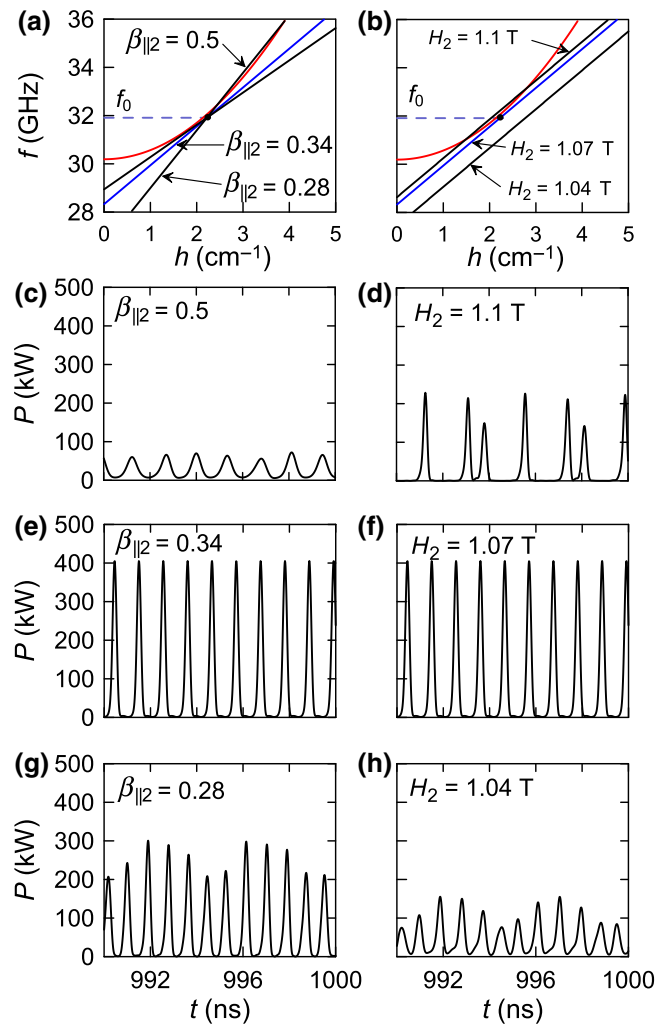


FIG. 6. Decrease in amplitudes of generated pulses and stability deterioration in the case of absorber parameter deviation from the grazing regime: variation in particles translational velocity (left column), variation in the guiding magnetic field H_2 (right column): (a),(b) dispersion characteristics; (c)–(h) profiles of the output signal for different parameters.

Note that in our numerical examples, the pulse spectrum bandwidth $\Delta\omega/\omega \sim 0.1$ in accordance with the amplifier bandwidth, which for helical gyro TWT is about 10%–15%. Such a relatively narrow band validates the slow-wave approximation used in the developed averaged model [ratio between the neglected and the retained terms in Eqs. (4) and (5) is of the order of 0.1]. The roundtrip time of the pulse in the feedback loop exceeds the pulse duration significantly, which corresponds to a large number of feedback-loop modes in the amplification band.

IV. 3D PIC SIMULATIONS OF KA-BAND MODE-LOCKED ELECTRON GENERATOR

The results of the studies based on the averaged approach are used as a benchmark for direct 3D PIC

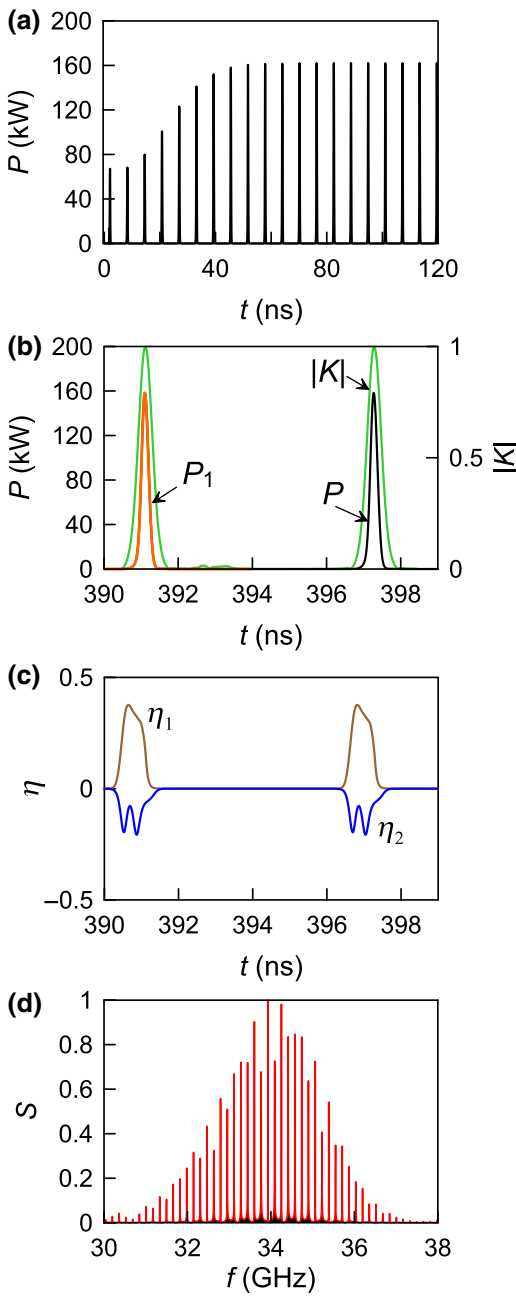


FIG. 7. The same as in Fig. 4 for generation in a hard-excitation regime.

simulations within the frame of the CST Studio Suite [37] software package. In the numerical model, the helical-waveguide amplifier and the cyclotron absorber are installed opposite to each other [see principle scheme in Fig. 1(b) and simulation model in Fig. 8]. From the cathode ends, both sections are bounded by resonance reflectors. Independent electron beams enter the simulation space from the left and right ends of the corresponding sections and, after interaction, deflect in a strong transverse magnetic field to the waveguide walls before polarizers.

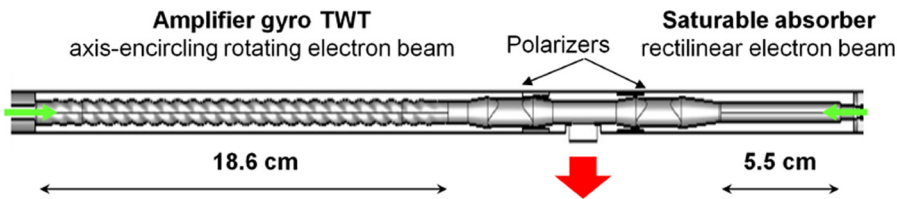
TABLE II. Parameters of amplifying and absorbing sections in hard-excitation regime of periodical generation.

| | Amplifier | Absorber |
|-----------------------|---------------------------------------|--------------------|
| Electron energy | 70 keV | 50 keV |
| Electron current | 8 A | 2.2 A |
| Pitch factor | 1.1 | 0 |
| Interaction length | 18.6 cm | 5.5 cm |
| Waveguide radius | 0.36 cm | 0.3 cm |
| Corrugation period | 1.15 cm | — |
| Corrugation amplitude | 0.06 cm | — |
| Operating mode | TE _{2,1} /TE _{-1,1} | TE _{-1,1} |

Parameters of sections correspond to those presented in Table II.

In both sections of the microwave mode-locked generator, the electron beams interact with co-traveling circularly polarized waves, while the counter-traveling waves propagate almost without interaction. For simulations of the branching of the electromagnetic power out to the load, the system of two polarizers and a polarization-selective coupler are used. Each polarizer represents a waveguide component having a circular cross section at the left-hand side, which gradually transforms along the z axis into the elliptical cross section in the middle and then back to the circular cross section at the right-hand side. The polarizers are oriented in such a way that in the space between them the counterpropagating waves have a linear polarization orthogonal to each other [see Fig. 1(b)]. Thus, the amplified signal in the form of a circularly polarized TE_{-1,1} mode enters the first polarizer, after passing through which the mode polarization changes from the circular to the linear one with E field oriented along the y axis. This y -polarized wave passes through the second polarizer, which converts it back to the circularly polarized wave. In the absorbing section this wave propagates without interaction in the backward direction to the electrons' motion. Then, after reflection, the signal becomes co-propagating and synchronously interacts with the absorbing electron beam. After exiting the absorber, the circularly polarized signal passes through the polarizer, which converts it into x -polarized TE_{1,1} mode. During this pass, a certain part of the wave power is outcoupled by a directional coupler. This system as a whole corresponds to the principal scheme shown in Fig. 1(a), where the radiation output of the microwave mode-locked generator is located after the absorber.

Results of PIC simulations presented in Fig. 9 confirm the practical feasibility of the chosen concept of a microwave mode-locked generator. The hard excitation modes are observed with a peak power of generated pulses from 120 to 150 kW and pulse duration of 300 ps, which is in good agreement with results predicted based on the developed averaged model (Sec. III). Note that the coherence of pulses (the time stability of the phase of microwave



oscillations) is maintained throughout the whole simulation time 300 ns, in spite of some variations in the amplitude of the generated pulses. As a result the radiation spectrum represents a so-called “frequency comb” [see Fig. 9(b)]. Note that the simulations within the averaged model show that the variations in pulses’ amplitudes can be eliminated by means of fine tuning of parameters.

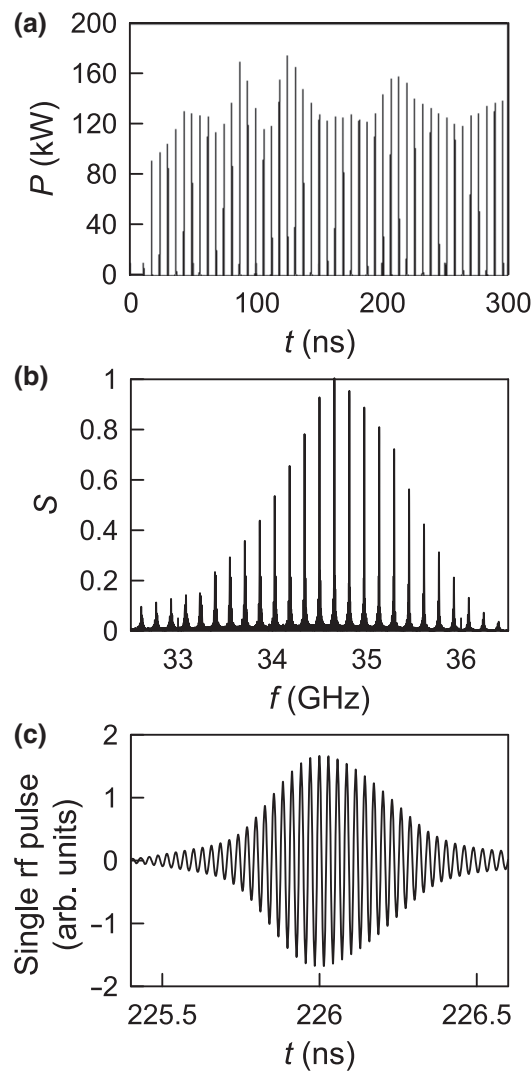


FIG. 9. Results of 3D PIC simulations. Hard-excitation mode is shown, when generation is initiated by a 20 kW, 10 ns pulse: (a) output power versus time; (b) radiation spectrum; (c) instant value of electrical field in a single rf pulse at a shorter time base.

FIG. 8. 3D PIC computer model of a microwave mode-locked generator, which is based on a helical-waveguide gyro TWT and a resonance cyclotron absorber.

However, in PIC simulations such an optimization requires significant computational resources.

V. CONCLUSION

Thus, based on a time-domain averaged model supported by direct PIC simulations, we demonstrate that a periodic train of powerful subnanosecond microwave pulses can be generated in an electron generator comprising a gyrotron traveling-wave tube with a helically corrugated waveguide and a cyclotron resonance saturable absorber with an initially rectilinear electron beam. At present, the considered type of microwave mode-locked generator is under development at the Institute of Applied Physics RAS (Nizhny Novgorod, Russia).

Note in conclusion that the considered scheme of microwave ultrashort pulse generators with passive mode locking is rather universal and can be based on a wide class of electron amplifiers including, besides gyro TWTs with regular and helical waveguides, also Cherenkov traveling-wave tubes, FELs, etc. Correspondingly, the broadband microwave pulses with a power level from kilowatts to multigigawatts can be generated from centimeter to submillimeter wavelength ranges. Using cyclotron resonance absorbers based on electron beams allows for significantly higher peak power in comparison with solid-state-based generators.

ACKNOWLEDGMENTS

This work is sponsored by Russian Scientific Foundation (RSF), Project No. 19-79-30071.

-
- [1] M.Yu. Tretyakov, M. A. Koshelev, I. N. Vilkov, V. V. Parshin, and E. A. Serov, Resonator spectroscopy of the atmosphere in the 350–500 GHz range, *J. Quant. Spectrosc. Rad. Trans.* **114**, 109 (2013).
 - [2] A. F. Krupnov, M.Yu. Tretyakov, G.Yu. Golubyatnikov, A. M. Schitov, S. A. Volokhov, and V. N. Markov, Technique of broadband measurements of frequency conversion efficiency for each harmonique in frequency multipliers up to terahertz range, *Int. J. of IR and MM Waves* **21**, 343 (2000).
 - [3] V. V. Parshin, M.Yu. Tretyakov, M. A. Koshelev, and E. A. Serov, Modern resonator spectroscopy at submillimeter wavelengths, *IEEE Sens. J.* **13**, 18 (2013).
 - [4] D. A. G. Deacon, L. R. Elias, J. M. J. Madey, G. J. Ramian, H. A. Schwettman, and T. I. Smith, First Operation of a Free-Electron Laser, *Phys. Rev. Lett.* **38**, 892 (1977).

- [5] D. Oepts and W. B. Colson, Phase locking in an infrared short-pulse free-electron laser, *IEEE J. Quantum Electron.* **26**, 723 (1990).
- [6] W. B. Colson, C. Pellegrini, and A. Renieri, in *Laser Handbook*, edited by W. B. Colson, C. Pellegrini, and A. Renieri (North Holland Publishing Co, Amsterdam, 1990), Vol. 6, pp.528.
- [7] A. H. McCurdy, Nonlinear theory of large-signal mode locking in a gyrotron oscillator, *Appl. Phys. Lett.* **66**, 1845 (1995).
- [8] E. Jerby and G. Bekefi, AM mode-locking of a free-electron laser oscillator, *IEEE J. Quantum Electron.* **29**, 2845 (1993).
- [9] E. Jerby, G. Bekefi, and T. Hara, Mode-locked free-electron laser oscillator, *Nucl. Instrum. Methods Phys. Res.* **318**, 114 (1992).
- [10] G. G. Denisov, S. V. Kuzikov, and A. V. Savilov, Q-switching in the electron backward-wave oscillator, *Phys. Plasmas* **18**, 103102 (2011).
- [11] H. A. Haus, Mode-locking of lasers, *IEEE J. of Select Topics in Quant. Electron.* **6**, 1173 (2000).
- [12] T. Brabec and F. Krausz, Intense few-cycle laser fields: Frontiers of nonlinear optics, *Rev. Mod. Phys.* **72**, 545 (2000).
- [13] R. Paschotta, *Field Guide to Laser Pulse Generation* (SPIE Press, Bellingham, WA, 2008).
- [14] T. Brabec, Ch. Spielmann, P. F. Curley, and F. Krausz, Kerr lens mode locking, *Opt. Lett.* **17**, 1292 (1992).
- [15] B. S. Collings, M. L. Mitchell, L. Boivin, and W. H. Knox, A 1021 channel WDM system, *IEEE Photon. Technol. Lett.* **12**, 906 (2000).
- [16] P. J. Winzer, D. T. Neilson, and A. R. Chraplyvy, Fiber-optic transmission and networking: The previous 20 and the next 20 years [invited], *Opt. Express* **26**, 24190 (2018).
- [17] A. Schliesser, N. Picqué, and T. W. Hänsch, Mid-infrared frequency combs, *Nat. Phot.* **6**, 440 (2012).
- [18] T. M. Jeong and J. Lee, Femtosecond petawatt laser, *Ann. Phys. (Berlin)* **526**, 157 (2014).
- [19] V. V. Lozhkarev, G. I. Freidman, V. N. Ginzburg, E. V. Katin, E. A. Khazanov, A. V. Kirsanov, G. A. Luchinin, A. N. Mal'shakov, M. A. Martyanov, O. V. Palashov, A. K. Poteomkin, A. M. Sergeev, A. A. Shaykin, and I. V. Yakovlev, Compact 0.56 petawatt laser system based on optical parametric chirped pulse amplification in KD*P crystals, *Laser Phys. Lett.* **4**, 421 (2007).
- [20] N. S. Ginzburg, G. G. Denisov, M. N. Vilkov, I. V. Zotova, and A. S. Sergeev, Generation of “gigantic” ultra-short microwave pulses based on passive mode-locking effect in electron oscillators with saturable absorber in the feedback loop, *Phys. Plasmas* **23**, 050702 (2016).
- [21] N. S. Ginzburg, G. G. Denisov, M. N. Vilkov, A. S. Sergeev, I. V. Zotova, S. V. Samsonov, and S. V. Mishakin, Generation of train of ultrashort microwave pulses by two coupled helical gyro-TWTs operating in regimes of amplification and nonlinear absorption, *Phys. Plasmas* **24**, 023103 (2017).
- [22] G. G. Denisov and S. J. Cooke, in *Digest 21st Int. Conf. Infrared and Millimeter Waves*, edited by M. von Ortenberg, H.-U. Mueller (P.AT2, Berlin, Germany, 1996).
- [23] G. G. Denisov, V. L. Bratman, A. D. R. Phelps, and S. V. Samsonov, Gyro-TWT with a helical operating waveguide: New possibilities to enhance efficiency and frequency bandwidth, *IEEE Trans. Plasma Sci.* **26**, 508 (1998).
- [24] G. G. Denisov, V. L. Bratman, A. W. Cross, W. He, A. D. R. Phelps, K. Ronald, S. V. Samsonov, and C. G. Whyte, Gyrotron Traveling Wave Amplifier with a Helical Interaction Waveguide, *Phys. Rev. Lett.* **81**, 5680 (1998).
- [25] V. L. Bratman, A. W. Cross, G. G. Denisov, W. He, A. D. R. Phelps, K. Ronald, S. V. Samsonov, C. G. Whyte, and A. R. Young, High-gain Wide-Band Gyrotron Traveling Wave Amplifier with a Helically Corrugated Waveguide, *Phys. Rev. Lett.* **84**, 2746 (2000).
- [26] L. Zhang, W. He, K. Ronald, A. D. R. Phelps, C. G. Whyte, C. W. Robertson, A. R. Young, C. R. Donaldson, and A. W. Cross, Multi-Mode coupling wave theory for helically corrugated waveguide, *IEEE Trans. Microwave Theory Tech.* **60**, 1 (2012).
- [27] S. V. Samsonov, I. G. Gachev, G. G. Denisov, A. A. Bogdashov, S. V. Mishakin, A. S. Fiks, E. A. Soluyanova, E. M. Tai, Y. V. Dominyuk, B. A. Levitan, and V. N. Murzin, Ka-band gyrotron traveling-wave tubes with the highest continuous-wave and average power, *IEEE Trans. Electron Devices* **61**, 4264 (2014).
- [28] R. Kompfner, On the operation of the travelling wave tube at low level, *J. Brit. IRE* **10**, 283 (1950).
- [29] C. S. Kou, K. R. Chu, D. B. McDermott, and N. C. Luemann, Jr., Effective bandwidth and the Kompfner dip for cyclotron autoresonance maser amplifiers, *Phys. Rev. E* **51**, 642 (1995).
- [30] N. S. Ginzburg, G. G. Denisov, M. N. Vilkov, A. S. Sergeev, S. V. Samsonov, and I. V. Zotova, in *Proceedings of 43rd International Conference on Infrared, Millimeter, and Terahertz Waves, Nagoya, Japan* (2018).
- [31] A. V. Gaponov, M. I. Petelin, and V. K. Yulpatov, The induced radiation of excited classical oscillators and its use in high-frequency electronics, *Izv. VUZov Radiofizika* **10**, 1414 (1967).
- [32] N. S. Ginzburg, I. V. Zotova, A. S. Sergeev, V.Yu. Zaslavsky, I. V. Zhelezov, S. V. Samsonov, and S. V. Mishakin, Mechanisms of amplification of ultrashort electromagnetic pulses in gyrotron traveling wave tube with helically corrugated waveguide, *Phys. Plasmas* **22**, 113111 (2015).
- [33] G. S. Nusinovich, *Introduction to the Physics of Gyrotrons* (The Johns Hopkins University Press, Baltimore, 2004).
- [34] N. S. Ginzburg, N. A. Zavolsky, and G. S. Nusinovich, Theory of non-stationary processes in gyrotrons with low Q resonators, *Int. J. Electron.* **61**, 881 (1986).
- [35] N. S. Ginzburg, A. S. Sergeev, I. V. Zotova, and I. V. Zhelezov, Time-domain theory of gyrotron traveling wave amplifiers operating at grazing incidence, *Phys. Plasmas* **22**, 013112 (2015).
- [36] N. S. Ginzburg, A. S. Sergeev, and I. V. Zotova, Time-domain self-consistent theory of frequency-locking regimes in gyrotrons with low-Q resonators, *Phys. Plasmas* **22**, 033101 (2015).
- [37] <https://www.cst.com>